RSC Advances

ROYAL SOCIETY OF CHEMISTRY

www.rsc.org/advances

One-pot hydrothermal synthesis of hematite-reduced graphene oxide composites for efficient removal of malachite green from aqueous solution

Airong Liu*, Wen Zhou, Kaile Shen, Jing Liu, Xixi Zhang

State Key Laboratory for Pollution Control and Resource Reuse

College of Environmental Science and Engineering,

Tongji University, Shanghai, China, 200092

Abstract

The facile one-pot synthetic route to prepare a 3D graphene composition of hematite (α-Fe_2O_3)-reduced graphene oxide (rGO) hybrid materials has been reported. The α-Fe_2O_3-rGO materials exhibit excellent capacity to remove malachite green (MG) from water. The pristine suspension of graphene oxide (GO) from Hummers method mixed with $FeCl_3$ and urea in the solution, is in situ transformed into α-Fe_2O_3-rGO composites under hydrothermal condition. The morphology and structure of the α-Fe_2O_3-rGO composites are characterized using transmission electron microscopy and scanning electron microscopy analyses, X-ray diffraction, Raman

* Corresponding author: Tel: +86-21-6598-2684; Fax: +86-21-6598-3689.

E-mail address: liuairong@tongji.edu.cn (Airong Liu)

spectroscopy, X-ray photoemission spectroscopy, Fourier transform-infrared spectroscopy, etc. It is found that α-Fe_2O_3 nanoparticles with cubic shapes and the particles with the cubic side of 10-30 nm are uniformly distributed on the graphene layer. The application of α-Fe_2O_3-rGO materials for the removal of MG from the aqueous solutions is investigated. The Langmuir model is found to fit well with the experimental isotherm data, with a maximum adsorption capacity of 438.8 $mg.g^{-1}$ for MG dye. The MG adsorption process is controlled by the pseudo-second-order rate model. The excellent capacity of α-Fe_2O_3-rGO to remove MG from water is ascribed to the synergetic adsorptive effect between α-Fe_2O_3 and rGO**.** The research provides an attractive adsorbent for removing of the hazardous materials from wastewater.

1 Introduction

Dyeing effluent has attracted increasing attention because of their long-term environmental toxicity and public health damages.[1] Malachite green (MG), a kind of dyes, has been found to be useful in many industrial applications as an antifungal, antimicrobial and anti-parasitic agent in food industry, as a therapeutic agent in aquaculture, as well as a dye in silk, wool, jute, and leather cotton, paper and acrylic industries.[2,3] But MG has toxic effects to human cells and mutagenic and carcinogenic properties as well, like causing liver tumor formation, hepatic and renal tumors formation in rodents and reproductive abnormalities in rabbits and fish. Consequently, it is of importance for the removal of the dye MG from the wastewater. Various techniques have been employed to remove the dyes from the water, such as

advance oxidation, photocatalysis, adsorption, membrane filtration, and coagulation.[1, 3-7] However, the most convenient and effective method for the removal of dye molecule from aqueous solution is the adsorption technique. A number of materials including activated carbon, carbon nanotubes, clays, chitosan hydrogels, and others,[8-11] have been explored as effective sorbents for the removal of contaminants.

Graphene, a novel and interesting carbon material, has generated a great deal of interest in the scientific and technological industries since its discovery by Geim and Novoselov in 2004.[12] Graphene materials have shown great application potential in many fields, such as electronic devices, energy storage and conversion, water treatment and biosensors, etc.[13-23] The extremely large surface area (2,630 $m^2 . g^{-1}$) and flat structure, as well as the low-cost, large-scale production of functionalized graphene make them to be excellent candidate for adsorption.[24] However, it is generally difficult to maintain the large surface area, because of the strong van der Waals interaction between graphene layers.[25] One effective method to obtain graphene as an individual sheet in suspension is to functionalize the surfaces of the graphene sheets with nanoparticles (NPs). The inorganic NPs presented in 2D graphene composites prevent graphene aggregation, as well as maintain a high surface area.

Hematite (α-Fe_2O_3), as an n-type semiconductor (Eg = 2.1 eV), is the most stable iron oxide under ambient conditions.[26] Due to the environmentally friendly and highly stable properties of α-Fe_2O_3, it can provide an opportunity for the development of novel adsorbents by synthesizing the graphene-based α-Fe_2O_3 hybrid composites, which are expected to exhibit superior

performances. The intimate interaction between the rGO substrates and the α-Fe_2O_3 NPs creates synergistic effects, which could generate a superior performance for wastewater treatment.[27,28] Graphene-based materials have been successfully applied in the adsorption of some organic pollutants in the form of dyes, polycyclic aromatic hydrocarbons, and gasoline.[25,29] The NP-graphene hybrid combination may lead to novel properties that are different from those of the individual components and that maximize its practical use due to the combined advantages. [30, 31]

Herein, we report a facile one-pot synthetic route to prepare a 3D graphene composition of the α-Fe_2O_3-rGO, and we apply it as an adsorbent to remove MG from water. The morphology and structure of the α-Fe_2O_3-rGO composites is studied by transmission electron microscopy (TEM) , scanning electron microscopy (SEM) X-ray diffraction (XRD), Raman spectroscopy, X-ray photoemission spectroscopy (XPS), Fourier transform-infrared spectroscopy (FTIR), etc. It is proved that under the hydrothermal condition, GO is simultaneously reduced to graphene along with the homogeneous precipitation of nano-sized α-Fe_2O_3. Compared to GO and rGO, α-Fe_2O_3-rGO composites can be easily separated from the solution after adsorption. The as-synthesized adsorbents possess high efficiency in the adsorption of organic dyes due to α-Fe_2O_3 and GO sheets properties. Due to the high stable properties of α-Fe_2O_3 and GO sheets, the nano adsorbents have a good retention characteristics for pollutants adsorption .

2 Experimental

2.1 Synthesis of α-Fe_2O_3-rGO

A detailed description for the synthesis of the GO has been published elsewhere,[32] and the remaining GO was collected by drying the precipitate in a vacuum oven.

The α-Fe_2O_3-rGO composites are synthesized as in the following procedure by a one-pot hydrothermal method. First, 0.81 g (0.003 M) of $FeCl_3 \cdot 6H_2O$ and 1.08 g (0.0018 M) of urea are added to 20 mL of a 1.8 $mg \cdot mL^{-1}$ GO aqueous solution while stirring, and the above mixture is sonicated for 15 min at 25°C. After, it is transferred and sealed into a 100 mL Teflon-lined stainless steel autoclave, deionized water is added to about 80mL, it is heated at 180°C in an electric oven for 8 h, and then it is cooled to room temperature naturally. The resulting black product is centrifuged and washed with deionized water and absolute alcohol several times, and the α-Fe_2O_3-rGO composites are obtained through drying at 50°C in a vacuum oven for 3 h. For a comparison, the single nano α-Fe_2O_3 materials are prepared under the same condition except for the addition of the aqueous dispersion of the GO.

2.2 Preparation of MG aqueous solution

Stock solutions are prepared by dissolving an appropriate amount of MG powders in DI water and stored in the bottle. Before adsorption experiments, the stock solutions are diluted to the certain concentration.

2.3 Characterization

The morphologies and structures of the as-prepared α-Fe_2O_3-rGO nanocomposites are examined using TEM (JEOL TEM 2100 FXII) with selected area electron diffraction (SAED), XRD (Bruker D8 ADVANCE diffractometer with Cu Kα radiation), Raman spectroscopy (Jobin Yvon LabRam-1B, France), XPS (Thermo VG Scientific Sigma Probe spectrometer) and FTIR (Nciolet5700) spectra. UV-vis spectroscopy (Shimazu UV-3150 spectroscope) is used to determine the concentration of MG solution.

2.4 Adsorption experiments

The adsorption capacity of α-Fe_2O_3-rGO is evaluated by the removal of dye pollutants, such as MG. The initial and final concentrations of the MG solutions are determined by a UV-visible spectrophotometer at a wavelength of 620 nm (λ_{max}).

Adsorption kinetic experiments are conducted to determine the equilibrium time and the kinetic models of MG sorption by α-Fe_2O_3-rGO composites. A loading of 0.2 $g.L^{-1}$ α-Fe_2O_3-rGO composites is added to 100 mL of the MG solution (75 $mg.L^{-1}$). The suspension is put into the shaker. At certain time intervals, the sample is taken out to determine the concentration of the remaining MG by UV-vis spectroscopy. Finally, the relative dye adsorption (%) versus the adsorption time is determined.

Dye adsorption isotherms are determined at the initial pH (pH = 6.96) of the solution. The dosage of 0.2 $g.L^{-1}$ of the α-Fe_2O_3-rGO nano-adsorbents is

put into aliquots of 100 mL of the MG solution at concentrations of 75, 90 100, 105, 110 and 125 mg.L^{-1}. After shaking for 6 h, the concentration of the supernatant is measured by UV-vis spectroscopy.

3 Results and discussion

It is well known that urea can release CO_2 and OH^- when the temperature of the solution exceeds 80 °C,[33] and then, the Fe^{3+} ions react with the OH^- ions to form Fe $(OH)_3$ on the surface of the GO nanosheets. The α-Fe_2O_3 nanocubes are grown on the surfaces of the graphene nanosheets through a reduction process of the pristine GO to reduce graphene under a hydrothermal treatment at 180°C for 8 h. The involved reactions in the formation of α-Fe_2O_3 are suggested as follows:

$$CO(NH_2)_2 + 3H_2O \rightarrow 2NH_4^+ + CO_2 + 2OH^- \quad (1)$$

$$Fe^{3+} + 3OH^- \rightarrow Fe(OH)_3 \quad (2)$$

$$2Fe(OH)_3 \rightarrow \alpha - Fe_2O_3 + 3H_2O \quad (3)$$

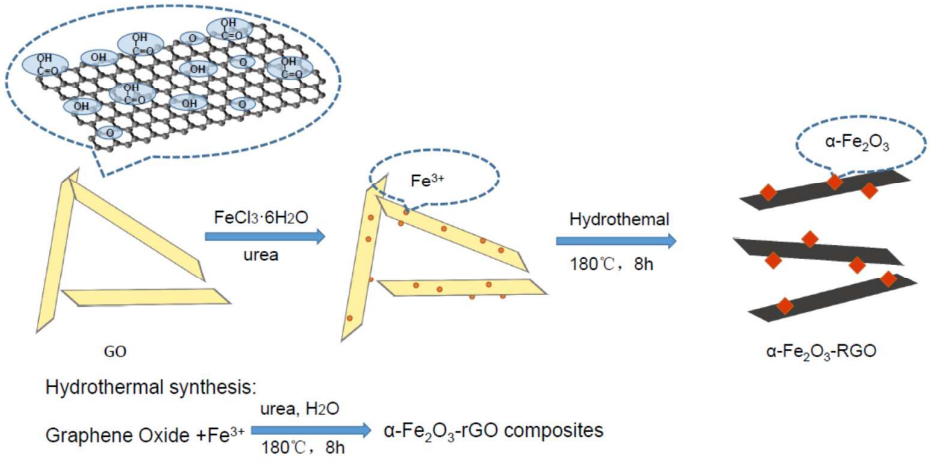

Fig.1. Schematic illustration of the one-pot synthesis of α-Fe_2O_3-rGO composites

The α-Fe_2O_3 nanocubes are intercalated into the graphene nanosheets, which effectively prevent the restacking of the as-reduced graphene nanosheets, and the hybrid α-Fe_2O_3-rGO composites are finally obtained.

3.1 Morphological and structural characterization of α-Fe_2O_3-rGO composites

3.1.1 TEM images of α-Fe_2O_3-rGO composites

The morphologies and structures of the α-Fe_2O_3-rGO composites are characterized by TEM. From the TEM image presented in Fig. 2a,b, it can be observed that the α-Fe_2O_3 particles are distributed homogeneously in the rGO sheets with cubic shapes. The HR-TEM picture shows that the side of the cubic particle is about 15 nm (Fig. 2c). Furthermore, no free or independent nanoparticles outside the graphene sheets indicate all of the nanoparticles are attached to the rGO. The SAED patterns (the insert of Fig. 2c) further prove the polycrystalline property of α-Fe_2O_3. The EDS spectrum (Fig. 2d) confirms the existence of Fe, C and O elements in the products, offers complementary evidence on the formation of α-Fe_2O_3-rGO composites.

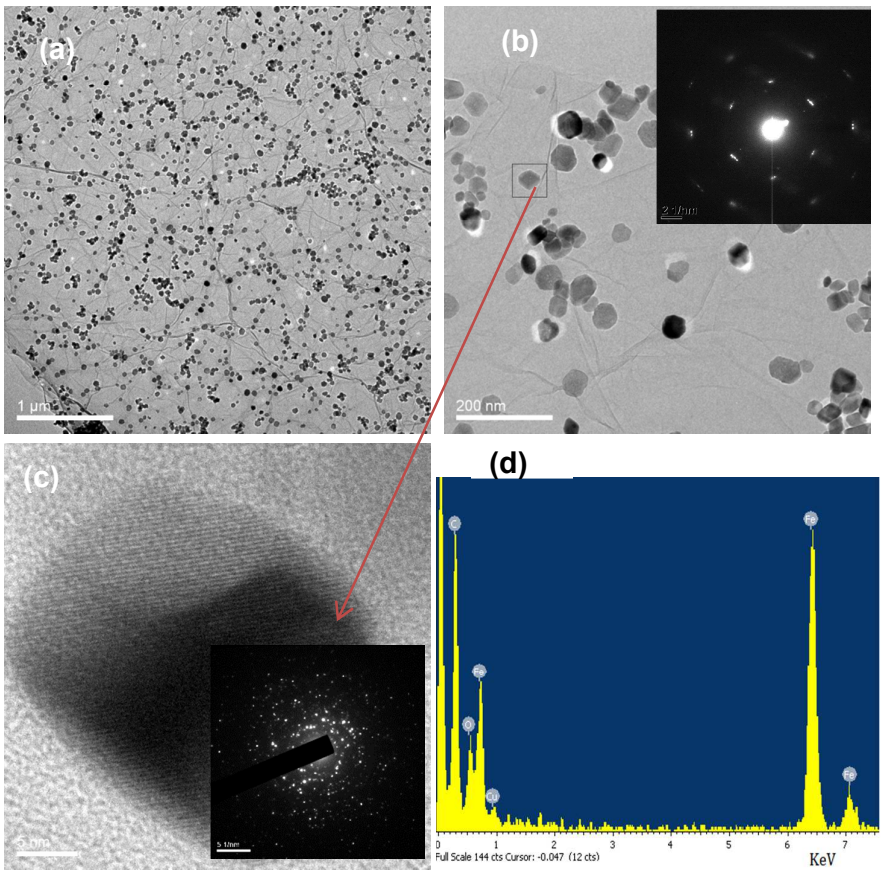

Fig. 2. TEM images of the α-Fe_2O_3-rGO composites (a, b) at different scales; the insert of (b) represents the SAED pattern of the graphene layer; (c) HR-TEM image and the SAED pattern (the insert) of a single α-Fe_2O_3 NP; (d) EDS analysis of the composites

3.1.2 XRD analysis

Fig. 3 shows the powder XRD patterns of graphite, α-Fe_2O_3, GO, and α-Fe_2O_3-rGO composites. The graphite shows a very sharp diffraction peak at 26.5°, corresponding to a d-spacing of 0.336 nm (d_{002}) (Fig. 2a). The oxidation treatment produces a decrease in the diffraction peak (002) intensity of

graphite and the appearance of the diffraction peak of the GO at 2θ=11.2, corresponding to the (001) interlayer spacing of 0.83 nm (Fig. 3b).[34] As well, α-Fe_2O_3-RGO shows peaks corresponding to α-Fe_2O_3 (JCPDS No.80-2377), [35] and a broad peak appears at 23.9° which is attributed to rGO [33].

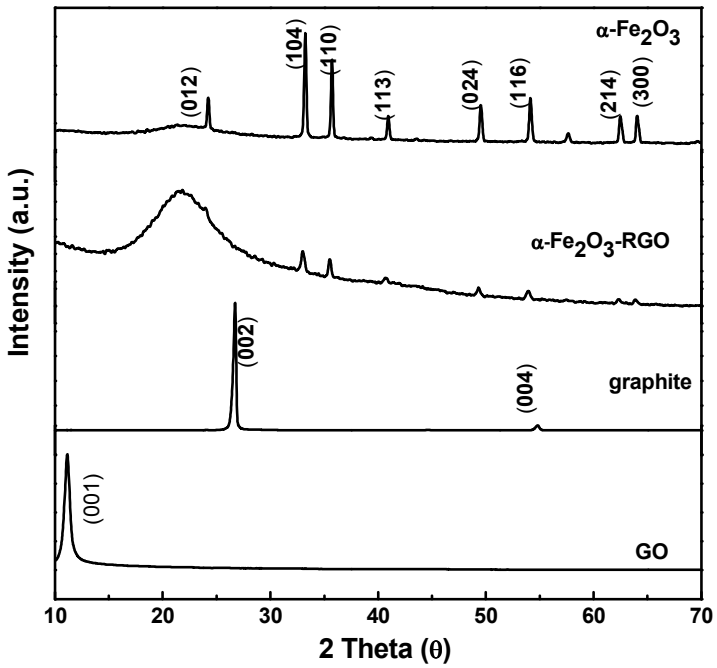

Fig.3. XRD patterns of graphite, GO, and α-Fe_2O_3-rGO.

3.1.2 Raman and FTIR spectroscopy analysis

The Raman spectra of the GO, rGO, and the α-Fe_2O_3-rGO in the range of 500–2,000 cm^{-1} are shown in Fig. 4. In Figure 4 (a), the Raman spectra (532 nm excitation) of α-Fe_2O_3-rGO displays two prominent peaks at ~1,330 and ~1,590 cm^{-1}, which correspond to the well-documented D-band and G-band, respectively.[34] It is well known that the G-band corresponds to the first-order

scattering of the E_{2g} mode observed for the sp^2 carbon domains, and the pronounced D-band is associated with structural defects, amorphous carbon, or edges that can break the symmetry and selection rule.[34,36] The ratio of the D-band intensity (I_D) to the G-band intensity (I_G) represents the disorder levels of the graphene. The G-band around 1,590 cm^{-1} and the D-band around 1,355 cm^{-1} are observed in the Raman spectrum of the GO. The I_D/I_G is usually used as a measure of the disorder. The I_D/I_G of GO is about 1.28. After hydrothermal reduction, the I_D/I_G of GO is increased to 1.42, indicating the presence of localized sp^3 defects with the sp^2 carbon network after a reduction in the exfoliated GO.

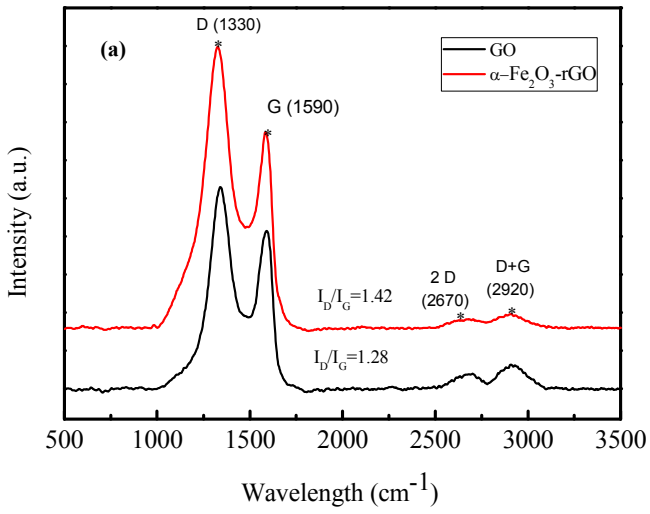

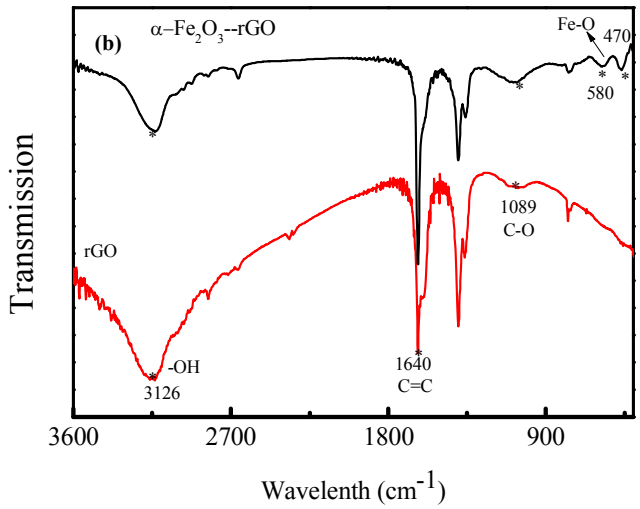

Fig. 4. Raman (a) and FTIR spectra (b) of GO and α-Fe_2O_3-rGO

Fig. 4 (b) shows the FTIR spectroscopy of the GO and α-Fe_2O_3-rGO. The adsorption band at 1,720 cm^{-1} is the characteristic band of the C=O groups in carbonyl and carboxyl moieties. The bands at 1,640 cm^{-1} are associated with the skeletal vibrations of the unoxidized graphitic domains (C=C).[36-38] The bands at 1,089 cm^{-1} are assigned to the C-O bonds, respectively. The band between 3,200 and 3,400 cm^{-1} is related to the O-H stretching vibration staring from OH^- in rGO and the water adsorbed on the surfaces of α-Fe_2O_3-rGO and rGO. The adsorption band at 470 cm^{-1} from the FTIR spectra can be assigned to the vibrations of the Fe-O with α-Fe_2O_3. The peak at 587 cm^{-1} can be credited to the lattice absorption of iron oxide, indicating the strong interaction of the NPs with the ester O.[37-39]

3.1.3 XPS analysis

The surface composition of the α-Fe_2O_3-rGO composites is further confirmed by XPS measurements. The chemical state of the element in α-Fe_2O_3-rGO is further investigated by XPS. The wide scan XPS spectrum (Fig. 5.) of α-Fe_2O_3-rGO shows photoelectron lines at binding energies of about 285, 530, and 711 eV, as attributed to C 1s, O1s, and Fe 2p, respectively. In the spectrum of Fe 2p (Fig. 5b), the peaks Fe 2p3/2 and Fe 2p1/2 are located at 710.9 and 724.6 eV, which is indicative of the formation of the α-Fe_2O_3 phase in the RGO matrix.[36,40] Three species may be attributed to the O 1s types of oxygen. The binding energy at 530.4 eV is due to the oxygen in α-Fe_2O_3. The oxygen in GO is around 532.6 eV. Deconvolution of the C 1s peaks of the composites show the co-presence of different oxygen types contained in the composite. The peak around 284.8 eV is attributed to the non-oxygenated C at 284.8 eV. The peaks at 286.2, 287.9, and 289.0 eV are due to the C-O bond, the carbonyl (C=O), and the carboxylate carbon (O-C=O), respectively. The C 1s spectra of α-Fe_2O_3-rGO shows mainly the non-oxygenated carbon (284.8 eV).

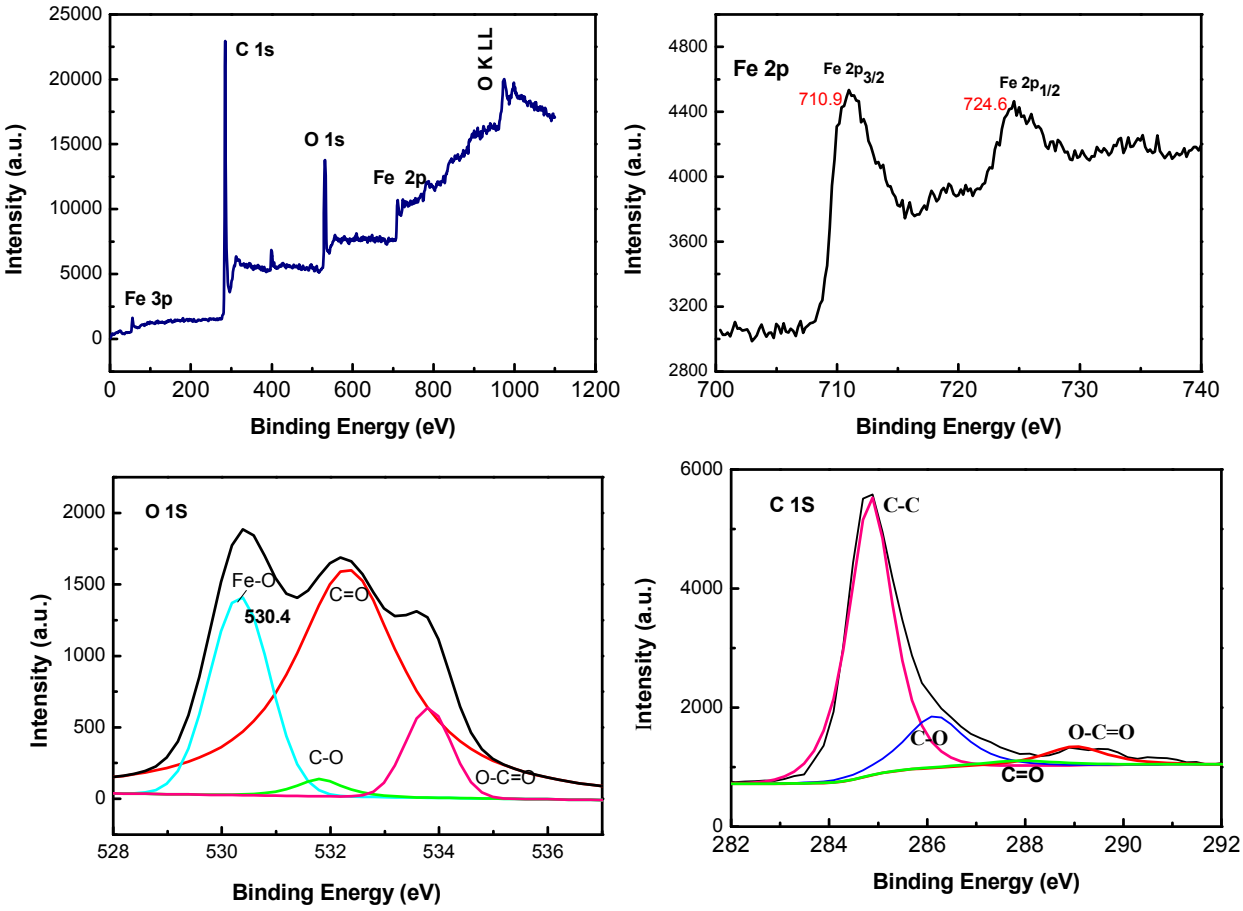

Fig.5. XPS spectra: (a) wide scan, (b) high-resolution Fe 2p spectra, (c) high-resolution O 1s spectra, and (d) C 1s spectra of α-Fe_2O_3-rGO composites

3.2 Application for the rapid removal of MG from water

After a 0.5 $g.L^{-1}$ loading of the materials is put into 30 $mg.L^{-1}$ of the MG solution, the UV-vis spectroscopy of the dye in the solution is measured after adsorption by the α-Fe_2O_3-rGO composite at a certain reaction interval. The results are shown in Fig. 6. The characteristic peak (620 nm) is observed from the starting solution of MG, which is similar to those reported previously.[1-3] After the α-Fe_2O_3-rGO composite is put into the MG solution, the intensity of

the MG adsorption peak decreases with the prolonged time. The reaction solution turns colorless gradually after 30 min.

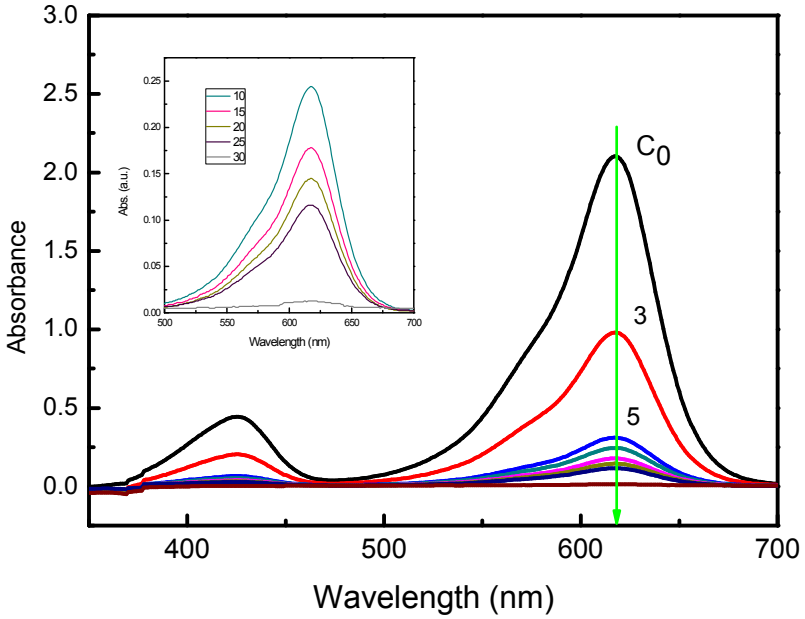

Fig.6. UV spectrum of MG dye solution (c_0=30 mg.L^{-1}) in the presence of α-Fe_2O_3-RGO (the loading of α-Fe_2O_3-rGO composites is 0.5 g.L^{-1}) at different time intervals (3-30 min).

As graphene has an extremely large, specific surface area that provides available adsorption sites, graphene or GO can be employed as an adsorbent for dye removal. MG molecules are easily adsorbed in the surface of graphene through the π--π conjugation, as based on its giant -π conjugation system, and the 2D-planar structure until the adsorption equilibrium is achieved.[1] Such adsorption increases the effective concentration of MG molecules significantly

near the surface of the α-Fe_2O_3-rGO materials. Second, based on the SEM, TEM, XPS analyses, graphene nanosheets can prevent the aggregation of α-Fe_2O_3. The α-Fe_2O_3 NPs uniformly distribute on the surface of graphene. Both α-Fe_2O_3 and graphene could play great roles in the coupled adsorption effect.

3.2.1 Analysis of adsorption kinetics

The adsorption efficiency of MG is calculated according to the following equation:

$$\text{Removal efficiency} = (1\text{-}C_t/C_0)\times 100\% \quad (4)$$

Where C_0 is the initial concentration of MG and C_t is the concentration of MG at the interaction time (min).

The adsorption kinetics has a great deal to say on the subject of the rate of uptake which effects the residence time at the solid-solution interface. There are several kinetic models to describe the adsorption mechanism. In this study, the kinetics of adsorption is explained by the pseudo-first-order and pseudo-second-order kinetic models. The pseudo-first-order rate equation suggested by Lagergren is presented as follows:

$$\frac{\mathrm{dq}}{\mathrm{dt}} = k_1(q_e - q) \quad (5)$$

Where q_e and q are the adsorption capacities at equilibrium and time t/min, respectively; and k_1/min^{-1} is the rate constant of pseudo-first-order adsorption. Integrating Eq 6 for q=0 at t=0 and q=q at t=t yields

$$\mathrm{q} = q_e(1 - e^{-k_1 t}) \quad (6)$$

The pseudo-second-order kinetic model can be described by Eq. (7).

$$\frac{t}{q_t} = \frac{t}{q_e} + \frac{1}{k_2 q_e^2} \quad (7)$$

Where k_2 is the pseudo-second-order rate constant ($g.mg^{-1}.min^{-1}$) and q_e and q_t are the dye sorption capacity at equilibrium (e) and time (t), respectively. A plot of t/q_t versus t yields the values of q_e and k_2. The initial adsorption rate V_0 ($mg.g^{-1}$) can be calculated using Eq. (8).

$$V_0 = k_2 q_e^2 \quad (8)$$

In the present work, the parameters of pseudo-first-order kinetic models are obtained by nonlineat regression, while the parameters of pseudo-second-order kinetic models are obtained by linear regression. The calculated kinetic parameters, their corresponding R^2 are given in Table 1.

Table 1. Adsorption Kinetic Parameters of MG on α-Fe_2O_3-rGO

model	Parameters	values
pseudo-first-order	q_e ($mg.g^{-1}$)	344.88
	K_1(min^{-1})	0.0283
	R^2	0.9016
pseudo-second-order	q_e ($mg.g^{-1}$)	395.26
	K_2($mg.g^{-1}.min^{-1}$)	8.06×10^{-5}
	V_0 ($mg.g^{-1}.min^{-1}$)	12.60
	R^2	0.9985

Figure 7 (a) shows the data for the adsorption of MG dye solutions by the α-Fe_2O_3-rGO over 6 h. Figure 7 (b) shows the experimental data, the predicted pseudo-first-order kinetics using the nonlinear method. Figure 7 (c) shows the experimental data using the pseudo-second-order kinetic model, which is based on the assumption that chemisorption is the rate-determining step.[1, 41-43] Observed in the Table 1, the larger value of the correlation coefficients (R^2>0.99) implies that the dye capture by the α-Fe_2O_3-rGO composite follows the pseudo-second-order kinetic mode. Compared to previous studies on dye adsorption, the parameters q_e, k_2, V_0 are much larger,[41-43] which demonstrates the large adsorption capacity of prepared nano-adsorbants. Both α-Fe_2O_3 and graphene could play great roles in the coupled adsorption effect.

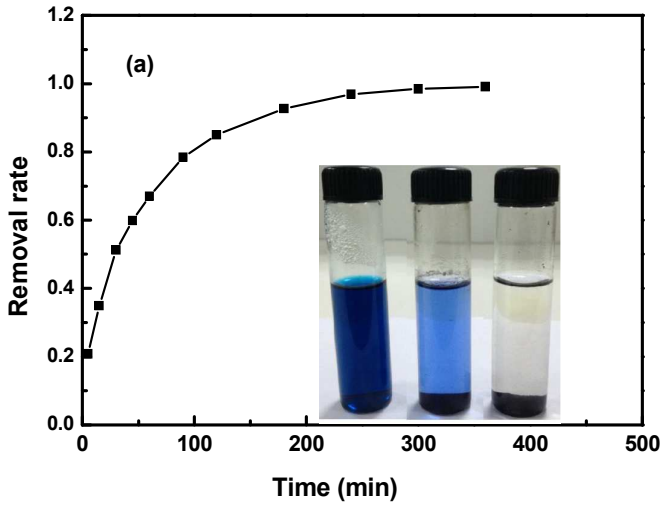

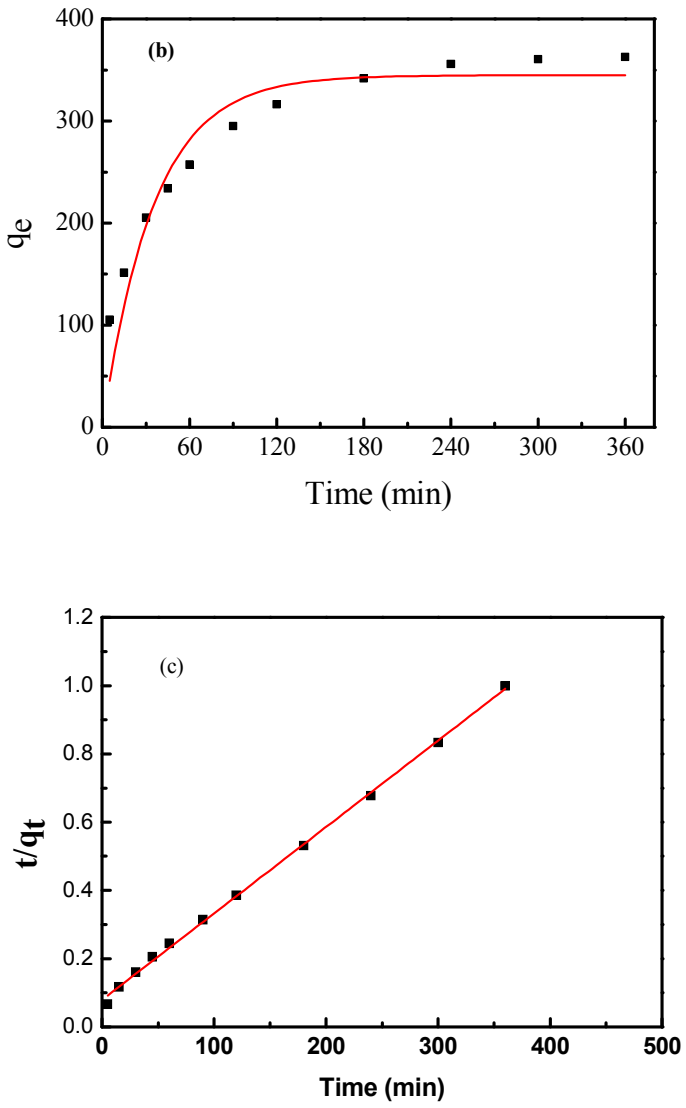

Fig. 7. Kinetic adsorption curve at room temperature (a), the pseudo-first-order kinetics (b) and the pseudo-second-order kinetics(c) of the adsorption of MG in the presence of α-Fe_2O_3-rGO .

3.2.2 Adsorption isotherms

The data obtained from the adsorption of MG are analyzed according to

the traditional models of adsorption. To obtain a better understanding of the sorption mechanisms and to quantify the sorption data, the Langmuir, Freundlich and Temkin models are used to simulate the experimental data. Correlation coefficient (R^2) values, which are used to determine the goodness of fit for the models, are 0.2997 for Temkin models and 0.2216 for Freundlich models (Figures not shown). The small values show the bad fitting for the above two models. The Langmuir isotherm model is used to describe the monolayer sorption process. Its form can be expressed by the following equation:

$$\frac{C_e}{q_e} = \frac{C_e}{q_{max}} + \frac{1}{K_L q_{max}} \quad (7)$$

Where q_{max} ($mg.g^{-1}$), the maximum sorption capacity, is the amount of MG at complete monolayer coverage, K_L ($L.mg^{-1}$) is the constant that relates to the energy of sorption, and q_e ($mg.g^{-1}$ of dry weight) is the equilibrium sorption capacity. Figure 8 shows Langmuir isotherms for MG adsorption. R^2 of the Langmuir model is 0.9985. The q_{max} values provide an approximate evaluation of the adsorption amount of MG on the hybride material，which is 438.8 $mg.g^{-1}$, a value much larger than identified in previous studies. It is reported that the q_{max} values of other adsorbents are dozen $mg.g^{-1}$ for the MG organic dye, [41-43] and the α-Fe_2O_3-rGO materials exhibit a high adsorption capacity in the aqueous solution. The synergetic effect between α-Fe_2O_3 and rGO enables the composites to have excellent adsorption capacity.

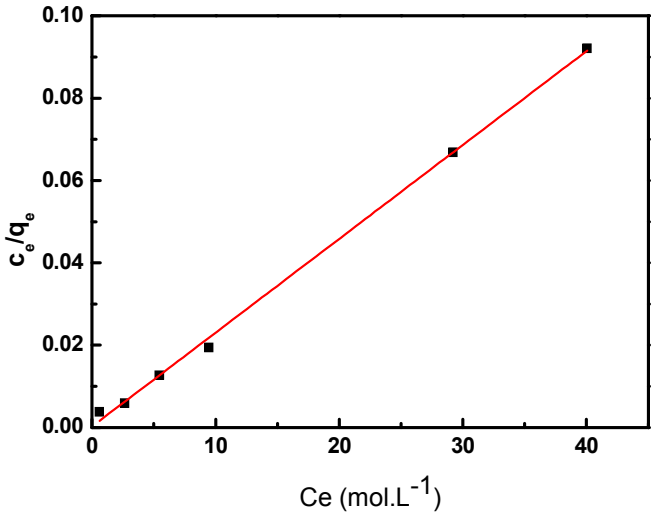

Fig. 8. Langmuir isotherms for MG adsorption

4 Conclusions

The α-Fe_2O_3-rGO composites are successfully prepared by the one-pot hydrothermal method with $FeCl_3$, urea, GO mixed together in the solution. The as-prepared poly-crystal α-Fe_2O_3 NPs with a relatively uniform size are embedded in the rGO layers and wrapped by rGO sheets to form the composites. The α-Fe_2O_3-rGO exhibits a high capacity to remove the MG in the solution. The adsorption process fits well the Langmuir isotherm, and the maximum adsorption capacity q_{max} values of MG is 438.8 mg.g^{-1}. The MG adsorption process is controlled by the pseudo-second-order rate model. The obtained nanomaterial is non-hazardous to the environment and practically usable for the removal of contaminants from water.

Acknowledgments

Research described in this work has been partially supported by the National Science Foundation of China (NSFC Grants 21277102, 21003151) and the Fundamental Research Funds for the Central Universities (20123211). The authors also thank Jinhao Han for his contribution in the revising text.

Notes and references

1. H. Tang, W. Zhou, L. Zhang, *J. Hazard. Mater.*, 2012, **209**, 218–225.
2. A. Afkhami, R. Moosavi, T. Madrakian, *Talanta*, 2010, **82**, 785–789.
3. K. Shashi, P. Deepak, S. Pardeep, D. Pooja, K. Amit, *Applied Catalysis B: Environ.*, 2014, **147**, 340–352.
4. B. Shi, G. Li, D. Wang, C. Feng, H. Tang, *J. Hazard. Mater.*, 2007, **143**, 567-574.
5. J. Lee, S. Choi, R. Thiruvenkatacharib, W. Shim, H. Moon, *Water Res.*, 2006, **40**, 435-444.
6. D. Mahanta, G. Madras, S. Radhakrishnan, S. Patil, *J. Phys. Chem. B* , 2008, **112**, 10153-10157
7. W. Chen, W. Lu, Y. Yao, M. Xu, *Environ. Sci. Technol.*, 2007, **41**, 6240-6245.
8. J. Rivera-Utrilla, M. Sánchez-Polo, V. Gómez-Serrano, P.M. Álvarez, M.C.M. Alvim-Ferraz, J.M. Dias, *J. Hazard. Mater.*, 2011, *1-3*, 1-23.
9. C. Lu, C. Liu, G.P. Rao, *J. Hazard. Mater.*, 2008, **151**, 239-246.
10. X. Li, Y. Li, Z. Ye, *Chem. Eng. J*, 2011, **178**, 60-68.
11. P. Castaldi, M. Silvetti, G. Garau, D. Demurtas, S. Deiana, *J. Hazard. Mater.*, 2015, **283**, 140-147.

12. K.S. Novoselov, A.K. Geim, S.V. Morozov, D. Jiang, Y. Zhang, S.V. Dubonos, I.V. Grigorieva, A.A. Firsov, *Science*, 2004, **306**, 666–669.
13. A.K. Geim, K.S. Novoselov, *Nat. Mater.*, 2007, **6**, 183–191.
14. F. Schedin, A.K. Geim, S.V. Morozov, E.W. Hill, P. Blake, M.I. Katsnelson, K.S. Novoselov, *Nat. Mater.*, 2007, *6*, 652–655.
15. L. Jue, D. Inhwan, T.D. Lawrence, M.W. Robert, L. Ilsoon, *ACS Nano*, 2008, **2**, 1230–1236.
16. A.R. Liu, S.M. Huang, *Sci China-Mech. Astron.*, 2012, **55**, 1163–1167.
17. S.K. Min, W.Y. Kim, Y. Cho, K.S. Kim, *Nat. Nanotechnol,* 2011, **6**, 162–165.
18. J.M. Yuk, J. Park, P. Ercius, K. Kim, D.J. Hellebusch, M.F. Crommie, J. Y. Lee, A. Zettl, A.P. Alivisatos, *Science*, 2012, **336**, 61–64.
19. F. Schwierz, *Nat. Nanotechnol*., 2010, **5**, 487–496.
20. S. Myung, J. Park, H. Lee, K.S. Kim, S. Hong, *Adv. Mater.*, 2010, **22**, 2045–2049.
21. G.X. Ni, Y. Zheng, S. Bae, C.Y. Tan, O. Kahya, J. Wu, B.H. Hong, K. Yao, B. Özyilmaz , *ACS Nano*, 2012, **6**, 3935–3942.
22. S.Y. Park, J. Park, S.H. Sim, M.G. Sung, K.S. Kim, B.H. Hong, S. Hong, *Adv. Mater.*, 2011, **23**, H263–H267.
23. T.D. Cohen, J.C. Grossman, *Nano Lett.*, 2012, **12**, 3602–3608.
24. W.H. Lee, J. Park, S.H. Sim, S. Lim, K.S. Kim, B.H. Hong, K. Cho, *J Am. Chem. Soc.*, 2011, **133**, 4447–4454.
25. M.J. Allen, V.C. Tung, R.B. Kaner, *Chem. Rev.*, 2010, **110**, 132−145.
26. X.L. Fang, C. Chen, M.S. Jin, *J. Mater. Chem.*, 2009, **19**, 6154–6160.

27. Y.J. Lin, G.B. Yuan, S. Sheehan, S. Zhou, D. Wang, *Energy Environ. Sci.*, 2011, **4**, 4862–4869.

28. D. Chen, G. Wang, S. He, J. Liu, L. Guo, M.S. Cao, *J. Mater. Chem.*, 2013, **1**, 5996–6003.

29. X. Yang, C.L. Che n, J.X. Li, G.X. Zhao, X.M. Ren, X.K. Wang, *RSC Adv.*, 2012, **2**, 8821–8826.

30. J. Zhu, T. Zhu, X.Z. Zhou, Y.Y. Zhang, X.W. Lou, X.D. Chen, *Nanoscale*, 2011, **3**, 1084–1089.

31. X.J. Zhu, Y.W. Zhu, S. Murali, M.D. Stoller, R.S. Ruoff, *ACS Nano*, 2011, **5**, 3333–3338.

32. W.S. Hummers *,* RE. Offeman, *J. Am. Chem. Soc.*, 1958, **80**, 1339.

33. C. Gao, X.Y. Yu, R.X. Xu, J.H. Liu, X.J. Huang, *ACS Appl. Mater. Interfaces*, 2012, **4**, 4672–4682.

34. J. Su, M.H. Cao, L. Ren, C.J. Hu, *J. Phys. Chem. C*, 2011, **115**, 14469–14477.

35. J.B. Lian, X.C. Duan, J.M. Ma, P. Peng, T.J. Kim, W.J. Zheng, *ACS Nano*, 2009, **3**, 3749–3761.

36. V. Chandra, J. Park, Y. Chun, J.W. Lee, I.C. Hwang, K.S. Kim, *ACS Nano*, 2010, **4**, 3979–3986.

37. Tang H, G.J. Ehlert, Y. Lin, H.A. Sodano, *Nano Lett.*, 2012, **12,** 84–90.

38. G. Cheng, Y.L. Liu, Z.G. Wang, J.L. Zhang, D.H. Sun, J.Z. Ni, *J. Mater. Chem.*, 2012, **22**, 21998–22004.

39. W.J. Zhang, X.H. Shi, Y.X. Zhang, W. Gu, B.Y. Li, Y.Z. Xian, *J Mater Chem.*, 2013, **A 1**, 1745–1753.

40. Y. Xue, H. Chen, D. Yu, S. Wang, M. Yardeni, Q. Dai, Y. Liu, F. Lu, J. Qu,

L. Dai, *Chem. Commun.*, 2011, **47**, 11689–11691.

41. J.N. Tiwari, K. Mahesh, N.H. Le, K.C. Kemp, R. Timilsina, R.N. Tiwari, K.S. Kim, *Carbon*, 2013, **56**, 173–182.

42. J. Guo, R.Y. Wang, W.W. Tjiu, J. Pan, T.X. Liu, *J. Hazard. Mater.*, 2012, **225**, 63–73.

43. Z. Yang, S. Ji, W. Gao, C. Zhang, L. Ren, W.W. Tjiu, T.X. Liu, *J Colloid. Interf. Sci,* 2013, **408**, 25-32.

A table of contents entry

The α-Fe_2O_3-rGO materials prepared by one-pot hydrothermal condition exhibit excellent capacity to remove MG from water.